



**Fermi National Accelerator Laboratory**

**FERMILAB-Conf-93/381**

## **Hyperon Polarization and Magnetic Moments**

Joseph Lach

*Fermi National Accelerator Laboratory  
P.O. Box 500, Batavia, Illinois 60510*

December 1993

*Invited talk 3rd Rio de Janeiro Workshop on Relativistic Aspects of Nuclear Physics,  
Centro Brasileiro de Pesquisas Fisicas, Rio de Janeiro, Brazil, August 25-27, 1993*

## **Disclaimer**

*This report was prepared as an account of work sponsored by an agency of the United States Government. Neither the United States Government nor any agency thereof, nor any of their employees, makes any warranty, express or implied, or assumes any legal liability or responsibility for the accuracy, completeness, or usefulness of any information, apparatus, product, or process disclosed, or represents that its use would not infringe privately owned rights. Reference herein to any specific commercial product, process, or service by trade name, trademark, manufacturer, or otherwise, does not necessarily constitute or imply its endorsement, recommendation, or favoring by the United States Government or any agency thereof. The views and opinions of authors expressed herein do not necessarily state or reflect those of the United States Government or any agency thereof.*

# Hyperon Polarization and Magnetic Moments

Joseph Lach  
Fermilab

*3<sup>rd</sup> Rio de Janeiro Workshop  
on  
Relativistic Aspects of Nuclear Physics*

Centro Brasileiro de Pesquisas Físicas  
Rio de Janeiro, Brazil

August 25-27, 1993

# Hyperon Polarization and Magnetic Moments

Joseph Lach

Fermilab

## Abstract

Inclusively produced hyperons with significant polarization were first observed at Fermilab about seventeen years ago. This and subsequent experiments showed that  $\Lambda^0$  were produced polarized while  $\bar{\Lambda}^0$  had no polarization in the same kinematical region. This set the stage for many experiments which showed that most hyperons are produced polarized. Recent Fermilab experiments have showed that this phenomena is even more complex and theoretical understanding is still lacking. Nevertheless polarized hyperon beams have been an extremely useful experimental tool in measuring hyperon magnetic moments. Recently, magnetic moment precession of channeled particles in bent crystals has been observed. This opens the possibility of measuring the magnetic moments of charmed baryons.

The rich field of hyperon polarization has seen much experimental work in the last few years. It has also revealed significant challenges to our theoretical understanding of polarization mechanisms. Let me familiarize you with some of the basic properties of hyperons and some of the techniques that are used to study them.

The SU(3) combinations of the three lowest mass quarks (u, d, and s) to form baryons are depicted in Figure 1. Here I ignore, at least for the time being, the three heavier quarks (c, b, and t). I make the normal definition of hypercharge as the sum of baryon

number and strangeness. On the vertical scale I plot the hypercharge,  $Y$ , vs. the third component of the isotopic spin. Identifying electric charge as one half the hypercharge plus the third component of isotopic spin, I form the baryon octet and decuplet. The lowest mass spin 1/2 baryons are identified in Figure 1 as well as the lowest mass spin 3/2 baryons.

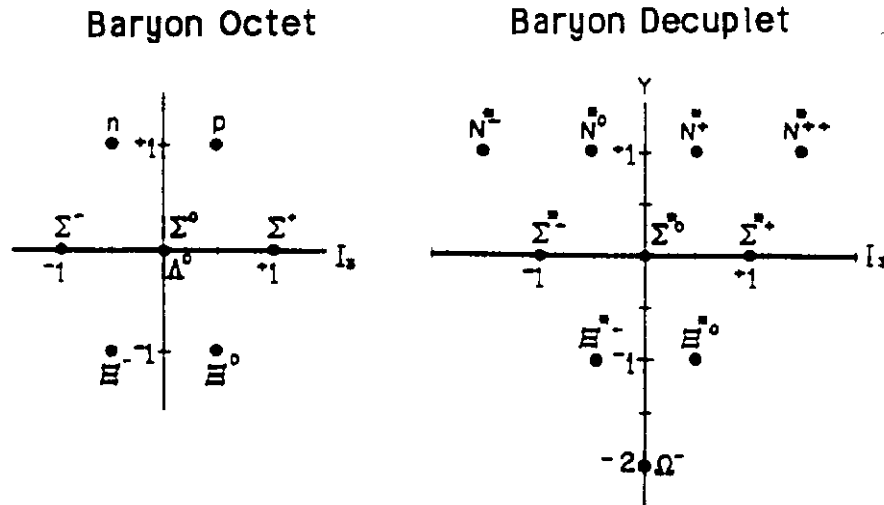


Figure 1.  
The Quark Structure of the Baryons

Within the octet all of the members are stable under the strong interactions; the rest - except for the proton - decay by way of the weak interactions. The  $\Sigma^0$  can also decay electromagnetically,  $\Sigma^0 \rightarrow \Lambda^0 \gamma$ ; the proton is stable. Among the lowest mass members of the decuplet only the  $\Omega^-$  does not decay strongly. Table 1 summarizes<sup>1</sup> the quark content and lifetimes of the long lived baryons; that is, those that do not have strong decays.

**Table 1 The Long Lived Baryons**

	Baryon	Quark Content	Mass MeV/c <sup>2</sup>	Lifetime Sec
<b>Octet</b>				
	p	uud	938.27	stable
	n	udd	939.57	889
Hyperons	$\Lambda^0$	uds	1115.63	$2.632 \times 10^{-10}$
	$\Sigma^+$	uus	1189.37	$7.99 \times 10^{-11}$
	$\Sigma^0$	uds	1192.55	$7.4 \times 10^{-20}$
	$\Sigma^-$	dds	1197.43	$1.479 \times 10^{-10}$
	$\Xi^0$	uss	1314.9	$2.90 \times 10^{-10}$
	$\Xi^-$	dss	1321.32	$1.639 \times 10^{-10}$
<b>Decuplet</b>				
	$\Omega^-$	sss	1672.43	$8.22 \times 10^{-11}$

There are a number of reviews describing hyperon beams and the physics programs that have utilized them<sup>2-5</sup>.

What are the essential elements of a hyperon beam?

- \*Start with a high energy proton beam
- \*Interact the beam in a small target to produce hyperons
- \*Select particles produced in the forward direction.
- \*Collimate in the other directions. Interact as many of the other secondary particles as practical, especially the pions before they can decay to muons.
- \*Magnetically select the desired charge and momentum
- \*Do all of the above in as short a distance as possible to maximize the number of hyperons that survive. This puts a premium on

- \*\*high magnetic fields
- \*\*high resolution detectors
- \*\*high energy

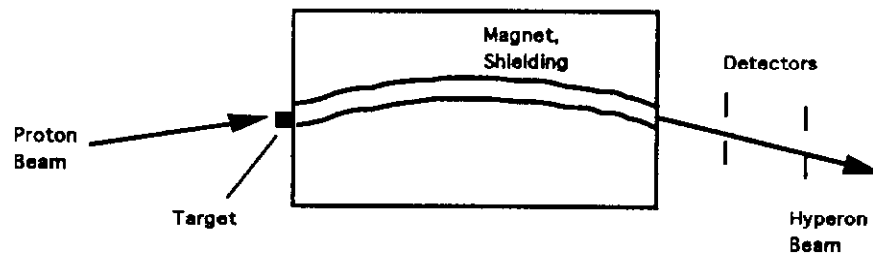


**Figure 2**  
Essential Elements of a Charged Hyperon Beam (plan view)

In Figure 2, we see the essential elements of a generic hyperon beam. The Fermilab hyperon beam in Fermilab's Proton Center has a 7m long magnet, the hyperon magnet<sup>6</sup>, with a vertical magnetic field of about 3.5 T. The inner portion of the magnet containing the channel is removable and can be fitted with a curved channel appropriate for a charged beam or a straight channel for a neutral beam. A set of magnets (not shown in Figure 2) upstream of the hyperon magnet allow for the angle of the proton beam impinging on the target to be varied either in the horizontal or vertical direction. This allows for the targeting angle to be varied between about  $\approx \pm 5$  mrad in either plane for 800 GeV incident protons. The transverse momentum,  $p_t$ , of the produced beam particle is just the product of the sine of the targeting angle and the hyperon momentum. Along with the Feynman  $x$  ( $x_F$ ), it is used to characterize a hyperon beam. To a good approximation,  $x_F$  is just the ratio of the secondary particle momentum divided by the incident proton momentum. The ability to change the targeting angle in both the horizontal and vertical planes is important since it allows one to control the direction of the hyperon polarization as will be discussed later.

Following the hyperon magnet is a set of high resolution spatial detectors. In the earlier beams these were spark chambers and then proportional chambers; now silicon strip detectors are used. In a recent configuration<sup>7</sup>, a Cu target of 0.5 mm full width in the horizontal plane coupled with 50  $\mu$ m pitch silicon strip detectors resulted in momentum resolution of  $\approx 0.25\%$  ( $\Delta p/p$ ) and angular resolution of  $\approx 10$   $\mu$ rad.

Early hyperon beams provided the first systematic measurements of hyperon fluxes and provided the "engineering" measurements needed for later beams. Figure 3 shows an early measurement<sup>8</sup> of these hyperon fluxes and a comparison with production of charged pions and kaons. This comparison is important since these are the contaminants to the hyperon beam and their numbers will usually limit rates in the apparatus designed to study hyperon properties.

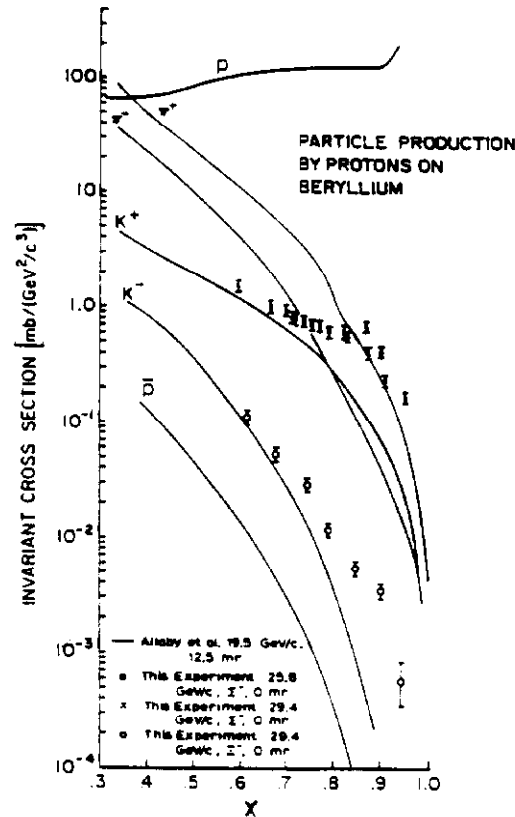
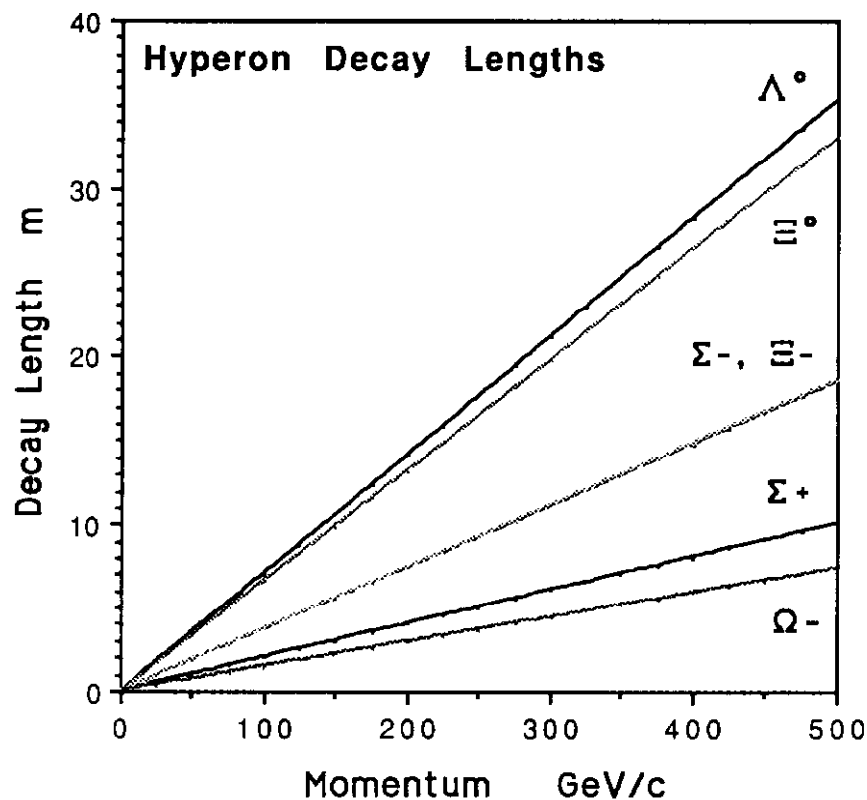


Figure 3  
Hyperon Production Comparison  
Cross section vs  $x_F$

Figure 3 deserves some comments. Plotted is the measured production cross section as a function of  $x_F$ . These yields have been corrected for decay losses and extrapolated back to the production target. One notes a surprising fact: at large  $x_F$  the yield of  $\Sigma^-$  is greater than that of  $\pi^-$ , and that of  $\Xi^-$  is greater



than that of  $K^-$ ! This demonstrated that hyperons are produced copiously at high energies and are  $\approx 10\%$  of all produced particles. It also showed the desirability of yet higher energy beams so that these high yields could be realized well downstream of the target. In Figure 4, I plot the hyperon decay lengths as a function of their momenta.



**Figure 4**  
Hyperon decay lengths as a function of momentum

Figure 5 is a diagram of the early CERN PS hyperon beam. That significant hyperon fluxes were available even at CERN PS energies<sup>9</sup> was beautifully demonstrated by the Cerenkov counter curve taken at the exit of their hyperon channel in Figure 5. The total distance from the target to the end of the Cerenkov counter was  $\approx 4\text{m}$ .

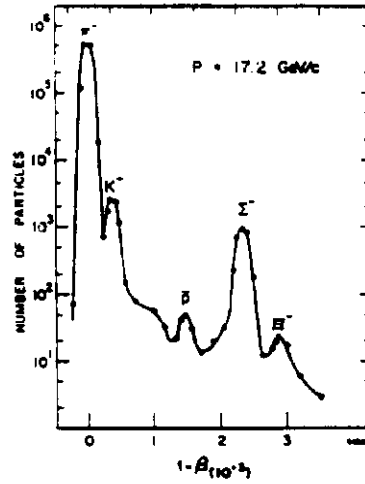
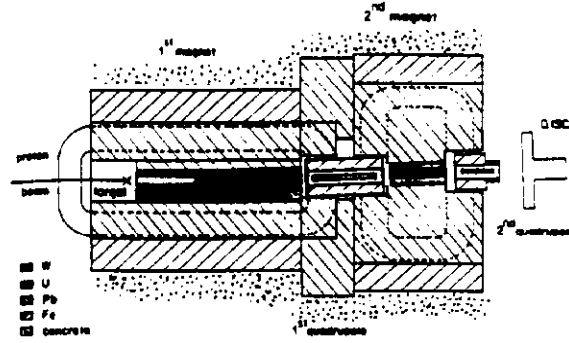


**Figure 5**

CERN PS Hyperon beam and  
velocity curve at 17.2 GeV/c showing the counting rate versus  $1-\beta$

The hyperons of the octet shown in Figure 1 all have spin  $1/2$ . Except for the  $\Sigma^0$ , which decays electromagnetically, all have their major decay modes mediated by the weak interactions. Because these weak decays do not conserve parity, information from the distribution of their decay products can be used to determine their spin direction. I illustrate this in Figure 6 where I schematically represent a polarized  $\Sigma^+$  decaying to  $\Sigma^+ \rightarrow p\pi^0$ . The center of mass distribution of the decay pion in this decay can be written as

$$I(\cos \theta) \approx 1 + \alpha P \cos \theta$$

where  $P$  is the  $\Sigma^+$  polarization and  $\alpha$  is characteristic of the weak decay properties of the particle.

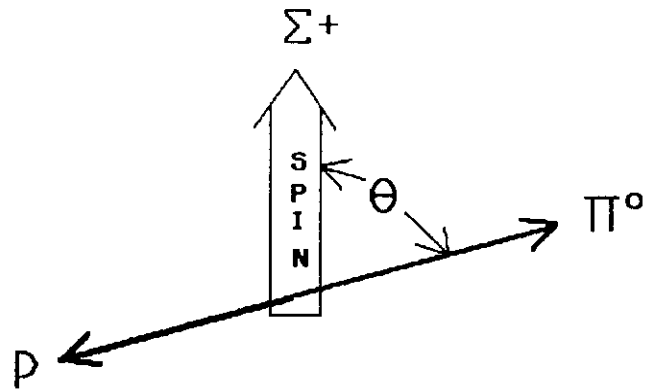


Figure 8

Decay of a polarized  $\Sigma^+ \rightarrow p\pi^0$ .

Table 2 Hyperon Decay Properties

Decay Mode	BR %	$\alpha$
$\Sigma^+ \rightarrow p\pi^0$	51.6	$-0.980 \pm 0.019$
$\Sigma^+ \rightarrow n\pi^+$	48.3	$0.068 \pm 0.013$
$\Sigma^- \rightarrow n\pi^-$	99.8	$-0.068 \pm 0.008$
$\Sigma^- \rightarrow ne^- \bar{\nu}$	0.1	$-0.519 \pm 0.104$
$\Lambda^0 \rightarrow p\pi^-$	64.1	$0.642 \pm 0.013$
$\Lambda^0 \rightarrow n\pi^+$	35.7	$0.65 \pm 0.05$
$\Xi^0 \rightarrow \Lambda^0 \pi^0$	100.	$-0.411 \pm 0.022$
$\Xi^- \rightarrow \Lambda^0 \pi^-$	100.	$-0.456 \pm 0.014$
$\Omega^- \rightarrow \Lambda^0 K^-$	67.8	$-0.026 \pm 0.026$
$\Omega^- \rightarrow \Xi^0 \pi^-$	23.7	$0.09 \pm 0.14$
$\Omega^- \rightarrow \Xi^- \pi^0$	8.6	$0.05 \pm 0.21$

The physics of the decay is contained in  $\alpha$ . If we just wish to measure a polarization or see the spin direction precess by a magnetic field we need not be concerned how nature gave us  $\alpha$ ; we

can just use it. Note that we measure asymmetries,  $A=\alpha P$ , the product of  $\alpha$  and  $P$ . We need to have them both non zero to measure a spin direction. Naturally, the larger the value of  $\alpha$ , the easier it is to measure  $A$  and hence the polarization.

Table 2 is a list<sup>1</sup> of some of the more important hyperon decay modes, branching ratios, and  $\alpha$  parameters for these decays.

From Table 2 we see that  $\alpha$  for the various decay modes can assume a wide range of values. The decay  $\Sigma^+ \rightarrow p\pi^0$  has  $\alpha$  near its maximum negative value, making it easy to measure the  $\Sigma^+$  polarization through this decay mode. The decay  $\Sigma^- \rightarrow n\pi^-$  has a small but clearly non-zero value of  $\alpha$  making it necessary to have a large data sample and good control of systematic errors to get a measurement of its polarization.

In decays such as  $\Xi^- \rightarrow \Lambda^0 \pi^-$ , where one also observes the subsequent decay,  $\Lambda^0 \rightarrow p\pi^-$ , information about the spin direction of the  $\Xi^-$  is also contained in the decay distribution<sup>3</sup> of the decaying  $\Lambda^0$ .

From Table 2, we see that for  $\Omega^-$  decays, the values of  $\alpha$  are all small and consistent with zero. In this case we must use the information from the subsequent  $\Lambda^0$  decay to determine the parent polarization. Note that one can still measure the  $\alpha$  parameters

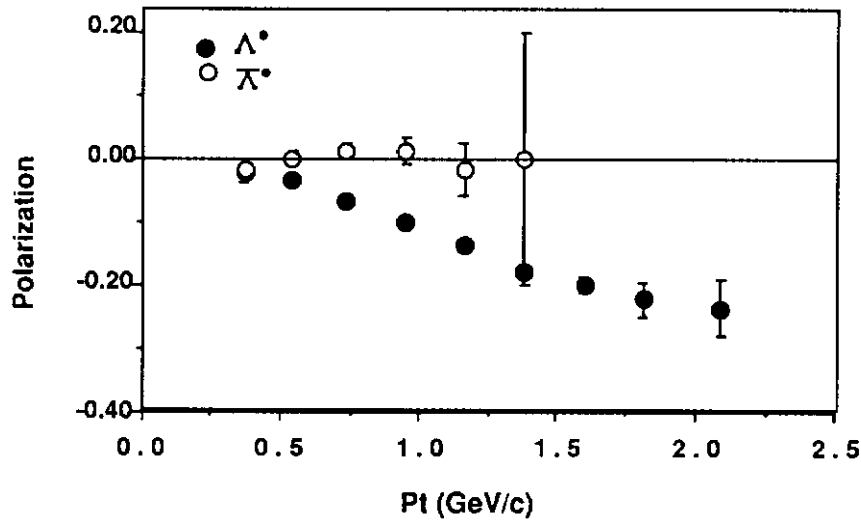


Figure 7  
Polarizations of particle  $\Lambda^0$  and  $\bar{\Lambda}^0$

for the  $\Omega^-$  decay even if the  $\Omega^-$  is not polarized<sup>5</sup>. This is further complicated by the fact that the  $\Omega^-$  has spin  $=3/2$ . However, similar procedures as for the  $\Xi^-$  decay have been developed<sup>10</sup>.

Significant  $\Lambda^0$  polarization was measured in the early Fermilab neutral hyperon beam<sup>11</sup>. Figure 7 shows data<sup>12</sup> for  $\Lambda^0$  and  $\bar{\Lambda}^0$  produced by 400 GeV protons. The polarization is plotted as a function of the transverse momentum,  $p_t$ , of the produced hyperon relative to the incident proton momentum. The  $\Lambda^0$  polarization was found to be zero in the forward direction (as required by rotational symmetry for production from an unpolarized beam and target) and decreased linearly to  $\approx -25\%$  at a transverse momentum ( $p_t$ ) of  $\approx 1.0$  GeV/c. These experiments also showed that the polarization had little dependence on the initial energy of the proton or the target material. We use the conventional sign definition<sup>13</sup> for the inclusive hyperon polarization: a positive polarization is in the same direction as the cross product of the incident beam direction with the produced hyperon direction.

The clear evidence (Figure 7) that  $\Lambda^0$  are produced with significant polarization came as a surprise. These polarizations have generally been attributed to peripheral mechanisms in which some of the proton valence quarks assimilate a strange quark from the sea to form a polarized hyperon.

The empirical conjecture that the more quarks incorporated from the sea reduces the produced hyperon polarization seemed to be confirmed by measurements of the polarization<sup>10,14-21</sup> of  $\Sigma^\pm$ ,  $\Xi^-$ , and  $\Omega^-$  hyperons. Figure 8 shows the measured polarizations of some other hyperons. Plotted here is the polarization as a function of the hyperon momentum at a fixed production angle. Since  $p_t = P_h \sin \theta$ , where  $P_h$  is the hyperon momentum and  $\theta$  the production angle, the horizontal axis is proportional to  $p_t$ . These are all produced by 400 GeV protons. Significant polarizations seem to be a general property of hyperon production at high energies.

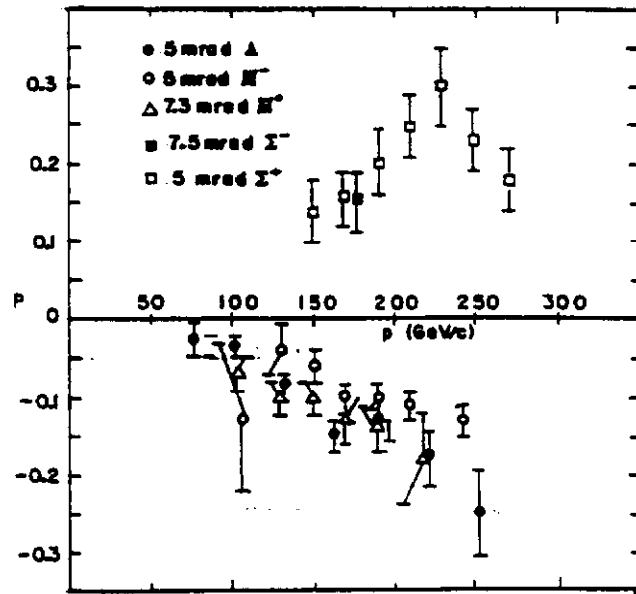


Figure 8

Polarization of other hyperons. Plotted is the polarization vs hyperon momentum at fixed angles. The horizontal axis is thus proportional  $p_t$ .

In our notation for the antiparticles, we adopt the convention that the written sign is the electrical charge of the particle under consideration. Thus, for the positively charged antiparticle of the  $\Xi^-$  we write  $\Xi^+$ , not  $\Xi^-$ .

In these interactions, the  $\Lambda^0$  is a leading particle and the  $\bar{\Lambda}^0$  is not. Might this be significant? One sees each of the hyperons being produced with polarization of  $\approx 10$ -20% at  $p_t \approx 1$  GeV/c. The fact that early experiments had shown  $\bar{\Lambda}^0$  to be unpolarized, where in the same kinematic range  $\Lambda^0$  was polarized, lent credence to the idea that polarization is a leading particle effect. This was supported by measurements<sup>10</sup> showing the  $\Omega^-$  to be unpolarized in this same kinematical region. Since the  $\Omega^-$  is composed of three strange valence quarks it contains none of the valence quarks of the incident proton.

However, recent data have cast great doubt on this picture. Measurement of the  $\Xi^+$  polarization by the Fermilab E756 group<sup>22</sup>, (Figure 9) shows  $\Xi^+$  to be polarized by about the same amount as the  $\Xi^-$ .

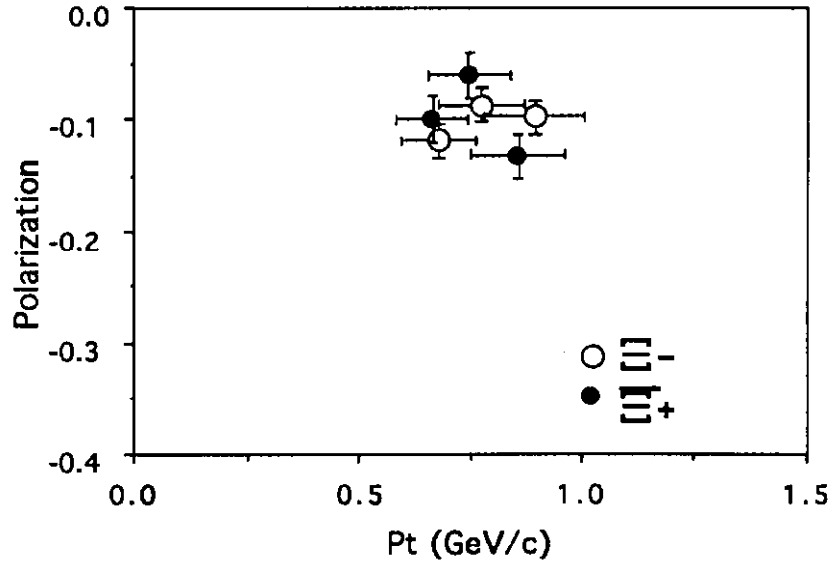


Figure 9  
 $\Xi^-$  and  $\Xi^+$  polarization

Recently our E761 group has measured<sup>23</sup> the polarization of 375 GeV/c  $\Sigma^+$  and  $\bar{\Sigma}^-$  produced by 800 GeV protons on a Cu target. The  $\Sigma^+$  was detected via its decay  $\Sigma^+ \rightarrow p\pi^0$  and the  $\bar{\Sigma}^-$  through its charge conjugate decay  $\bar{\Sigma}^- \rightarrow \bar{p}\pi^0$ . Figure 10ab shows the reconstructed  $\pi^0$  mass squared for the negative and positive beam. I show this to illustrate the capabilities of modern hyperon beams in statistics and resolution. In the positive data one clearly sees the rare radiative decay,  $\Sigma^+ \rightarrow p\gamma$ , whose study was the major goal of this experiment. Both this decay and the charge kaon decays are clearly visible but can be easily removed by making a selection on the missing mass.

Figure 11 shows the measured polarizations of  $\Sigma^+$  and  $\bar{\Sigma}^-$  as a function of  $p_t$ . In this data one sees that the  $\bar{\Sigma}^-$  is also produced with  $\approx 8\%$  polarization near  $p_t \approx 1$  GeV/c. A Be target was used in the E756  $\Xi^+$  data and a Cu target in E761. However, at least for  $\Lambda^0$  production, the nature of the target material does not seem to have a major effect on hyperon polarization. Pondrom<sup>3</sup> has a good summary of target material dependence of hyperon production and polarization data.

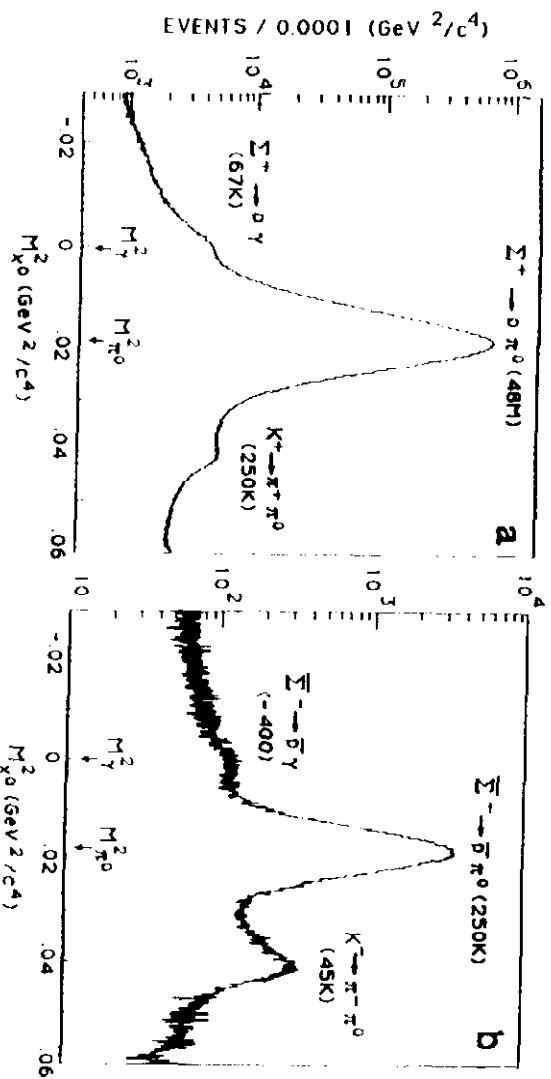


Figure 10

Event distributions of the mass squared of the missing neutral particle ( $X^\circ$ ) for the hypothesis  $\Sigma^+ \rightarrow pX^\circ$  for positive and negative beam candidates

This  $\Sigma^+$  data shows that the polarization increases with  $p_t$ , goes through a maximum near  $p_t = 1$  GeV/c and then decreases. This is the first time this decrease has been observed in a high energy hyperon polarization.

The data of Figure 11 show points taken with both horizontal and vertical targeting for  $\Sigma^+$  and  $\Sigma^-$ . In horizontal targeting, the incident beam direction is changed in the horizontal (H) plane producing polarization in the same plane (vertical) as the magnetic field of the hyperon magnet. Thus there is no spin rotation as the hyperons traverse the magnet. Targeting in the vertical (V) plane produces a polarization in the horizontal plane, perpendicular to the magnet field, thus producing maximum spin rotation as would be desired for measurement of a magnetic moment.



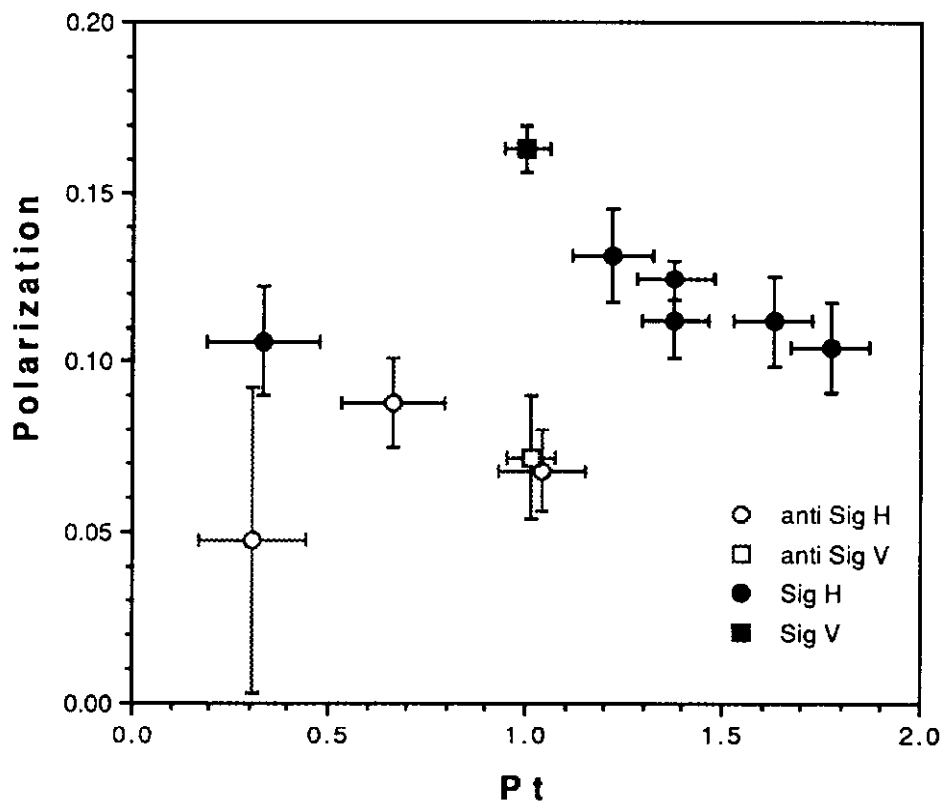


Figure 11  
 $\Sigma^+$  and  $\bar{\Sigma}^-$  polarization as a function of  $P_t$

This experiment demonstrated that  $\bar{\Sigma}^-$  hyperons are produced in high energy collisions with polarization of the same sign though of smaller magnitude than that of  $\Sigma^+$ . This observation is similar to the recent Fermilab results<sup>22</sup> which showed that both  $\Xi^-$  and  $\bar{\Xi}^+$  are polarized with about the same magnitude. This would indicate that the polarization of antihyperons is a common phenomenon, and we should now turn our attention to why the  $\bar{\Lambda}^0$  are not produced polarized.

Among the many proposed models for hyperon polarization<sup>24-27</sup>, let me mention two approaches to the polarization question - both involving similar leading particle effects. One is that of the Lund group<sup>28</sup> whose model assumes  $q\bar{q}$  pairs are produced from the sea via the breaking of a QCD string

but conserving local angular momentum. DeGrand and Miettinen<sup>29</sup> propose two simple rules: quarks which gain longitudinal momentum combine with spins down; quarks which lose longitudinal momentum combine with spins up. This is equivalent to a Thomas precession and a spin orbit coupling. Both models explain much of the hyperon data. The magnitudes of some of the polarizations are at odds with each of the models. A recent model using Regge pole approach<sup>30</sup> gives qualitatively good agreement with  $\Sigma^+$  polarization data. None of them can explain the polarizations of the antihyperons. Other models are discussed in a review by P. Kroll<sup>31</sup> which is recommended although it was done before the polarizations of the  $\Xi^+$  and  $\Xi^-$  were known.

Clearly the  $\Lambda^0/\bar{\Lambda}^0$ ,  $\Xi^-/\Xi^+$ , and  $\Sigma^+/\bar{\Sigma}^-$  systems exhibit a rich and challenging set of polarization phenomena that cry out for insightful ideas.

The fact that hyperons can be produced with significant polarization has allowed us to measure hyperon magnetic moments to remarkable precision. As I previously discussed one can control the hyperon polarization direction by the targeting angle of the incident proton beam. With this control one can produce the polarization perpendicular to the magnetic field direction so that significant spin rotation occurs as it passes through the hyperon targeting magnet (Figure 2).

Recent work has done much to improve the accuracy of the  $\Sigma^+$ ,  $\Xi^-$ ,  $\Omega^-$  magnetic moment measurements. The discovery that one can produce polarized  $\Xi^+$  and  $\Xi^-$  has allowed for the measurement of their magnetic moments. We note that the CPT theorem requires that the particle and antiparticle moments be the same in magnitude but opposite in sign. I will plot the negative of the antiparticle magnetic moments so that they can be more easily compared with the particle moments. Let me describe these new results.

Figure 12 shows the recent history<sup>14,15,32</sup> of measurement of the  $\Sigma^+$  magnetic moment. These spin precession effects are not small. For the case of  $\Sigma^+$  in E761, our most recent experiment<sup>32</sup>, we have a precession of the spin direction of 625°!

This result has served to clarify the discrepancy between the E497 and E620 measurements of the  $\Sigma^+$  magnetic moment and to produce a new world average. These are becoming precision measurements. The E761  $\Sigma^+$  magnetic moment measurement has a total error  $(\Delta\mu/\mu) = 0.21\%$  and the  $\Sigma^-$  of 1.5%. Note that this first measurement of the  $\bar{\Sigma}^-$  magnetic moment agrees very well (Figure 12) with the new  $\Sigma^+$  world average (with the opposite sign).

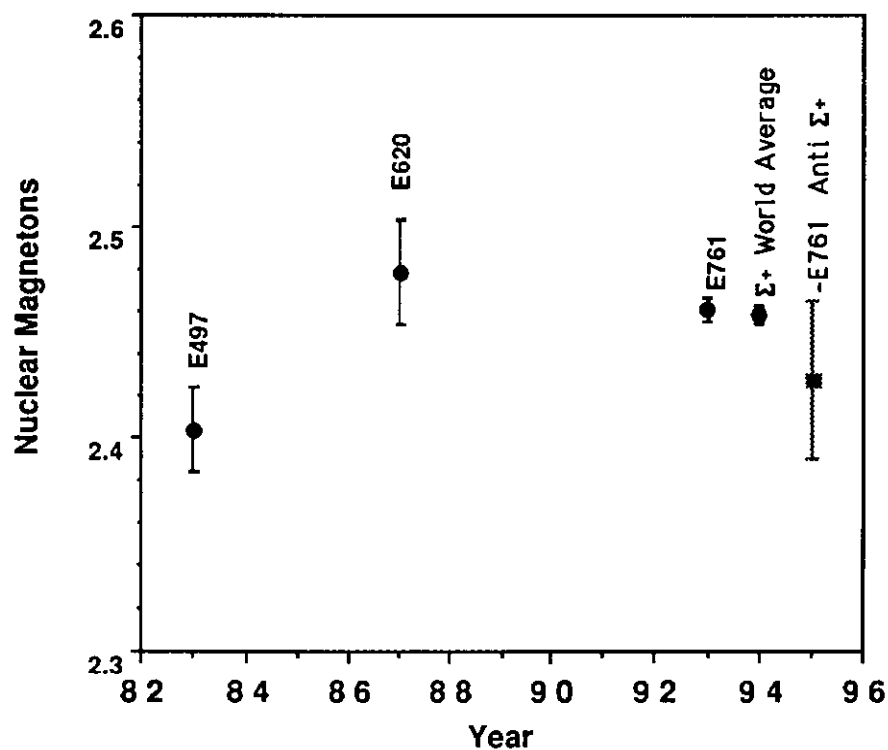


Figure 12  
 $\Sigma^+$  and  $\bar{\Sigma}^-$  Magnetic Moments measurements

Figure 13 shows the status of the  $\Xi^-$  and  $\bar{\Xi}^+$  magnetic moments measurements from the most recent experiments<sup>33,20,34,22</sup>. Again I point out the precision of the measurements and the agreement of the  $\bar{\Xi}^+$  with  $\Xi^-$  magnetic moments.

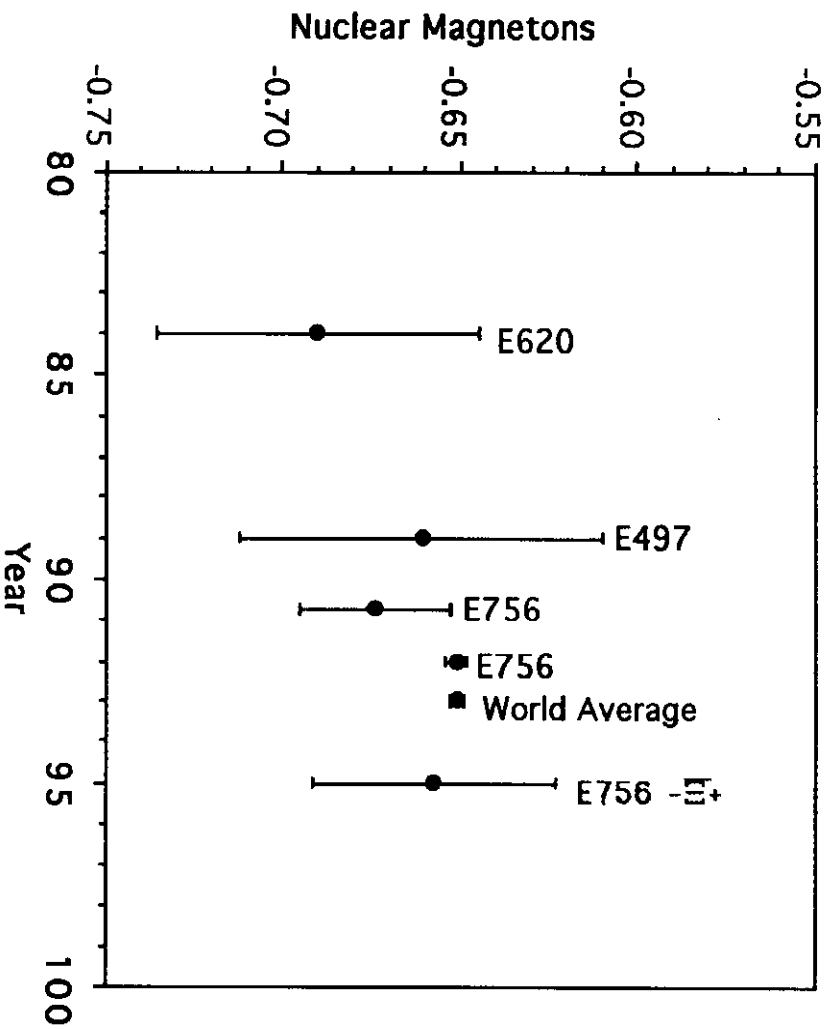


Figure 13

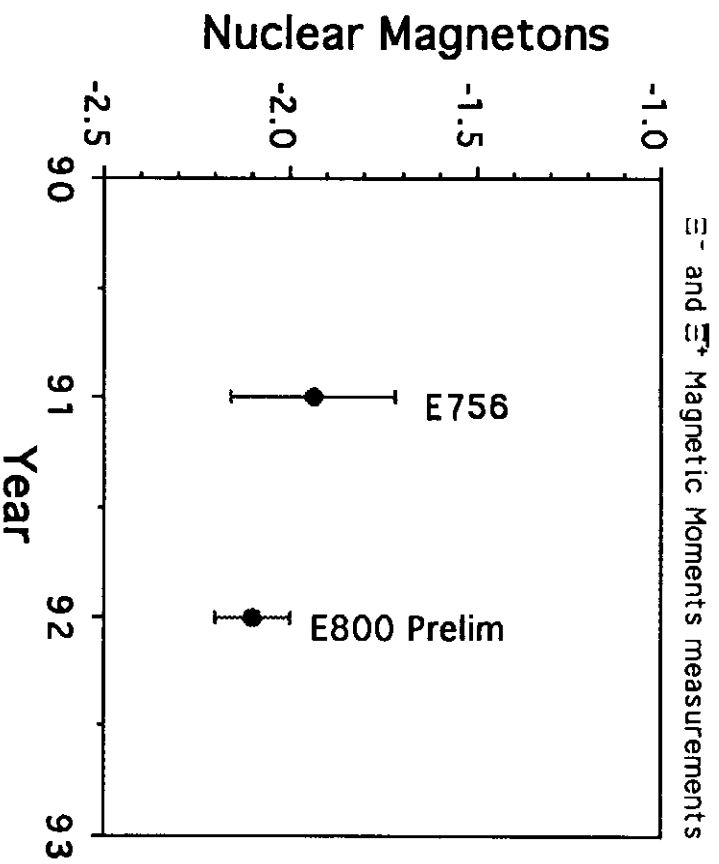


Figure 14

$\Omega^-$  Magnetic Moments measurements

Figure 14 shows the two existing measurements<sup>21,35</sup> of the  $\Omega^-$  magnetic moment. The Fermilab E800 result is still preliminary. The final result is expected to have a significantly reduced error.

We have now entered a remarkable period. Referring back to Figure 1, we see that reasonably good magnetic moment measurements now exist<sup>1</sup> for all of the baryons which do not decay strongly. This set of measurement could surely be improved but at this point, they are very much ahead of theoretical predictions. No new experiments are under way to improve on this data. It is the end of an era!

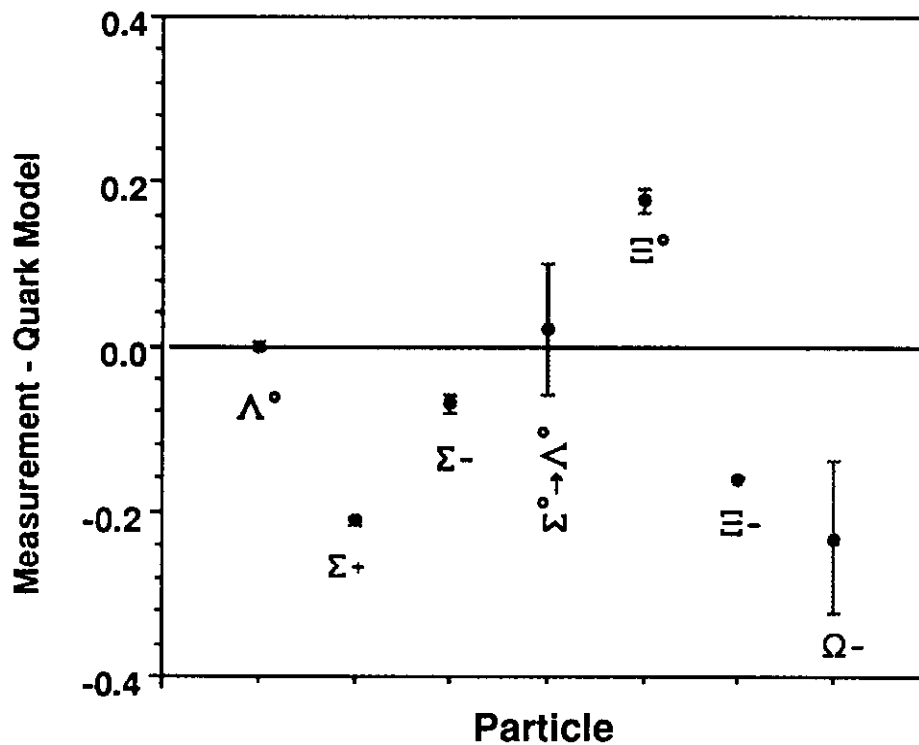


Figure 15.

Comparison between measured and Quark model predicted magnetic moments in nuclear magnetons

To put these measurements on a single graph, we can now compare these results with the simple quark model. In this model<sup>36</sup> we assume simple SU(6) wave functions and that only the

valence quarks contribute to the baryon magnetic moments. We plot in Figure 15 the deviations from the simple model of the measurements for all of the hyperons which are accessible to these kinds of experiments. No new neutral hyperon magnetic moment measurements have been done recently. Besides the magnetic moments, Figure 15 also includes the measurement of the  $\Sigma^+ \rightarrow \Lambda^0 \gamma$  transition moment. The rate of this purely electromagnetic decay is also predicted by the same formalism.

Let me conclude with a discussion of crystal channeling. The phenomenon of crystal channeling<sup>37,38</sup> has been of interest because of the very high effective magnetic fields that are involved. Figure 16 illustrates this phenomenon. Figure 16 depicts a crystal oriented so that a charged beam enters almost parallel to the crystal axis. A positively charged particle entering thus finds itself in a potential well formed by the positively charged arrays of nuclei. It is trapped -channeled- in this potential if the incident angle is near the crystal plane. If the angle is too large it passes through the crystal without being channeled as indicated in the same figure.

If one now bends the crystal as depicted in Figure 16b, one finds that one also bends the channeled beam<sup>37</sup>. From the momentum of the particle and the bend angle one realizes that the effective magnetic fields inside the crystal can be very large. Can these same large fields be used to precess the spin direction of a polarized beam? Fermilab E761, whose main goal was to look at hyperon radiative decays ( $\Sigma^+ \rightarrow p \gamma$  and  $\Xi^- \rightarrow \Sigma^- \gamma$ ), attempted to see this effect in a subsidiary experiment. A beam containing  $\Sigma^+$  hyperons is a good candidate for investigating this effect since they can be produced polarized and have a large decay asymmetry parameter ( $\alpha = -0.98$ ) for the common decay mode,  $\Sigma^+ \rightarrow p \pi^0$ . Hence, one can readily measure their spin direction from the decay distribution.

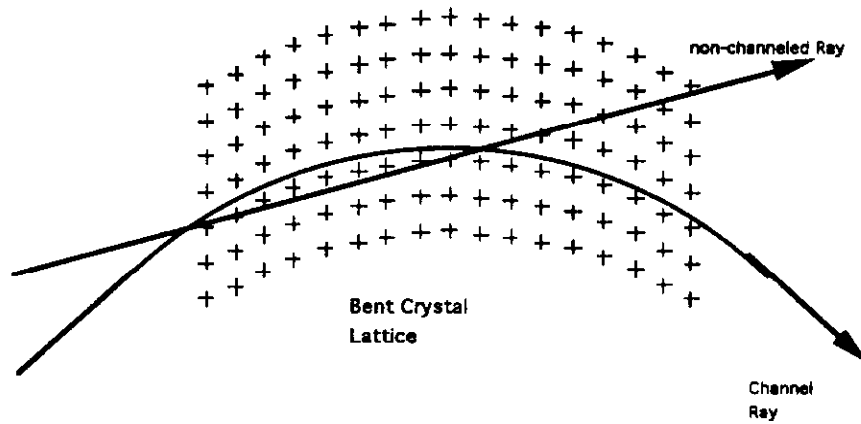
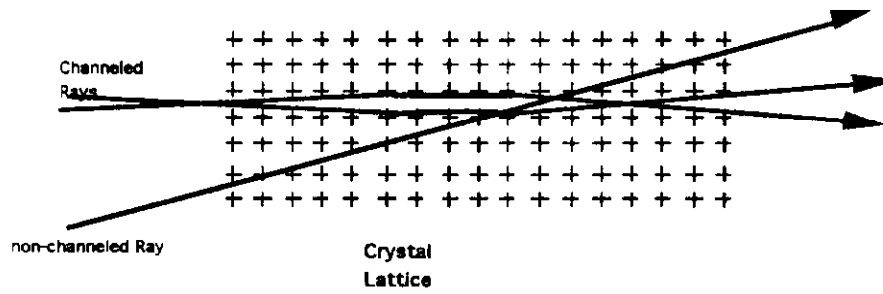


**Figure 16ab**  
Channeling in straight and bent crystal

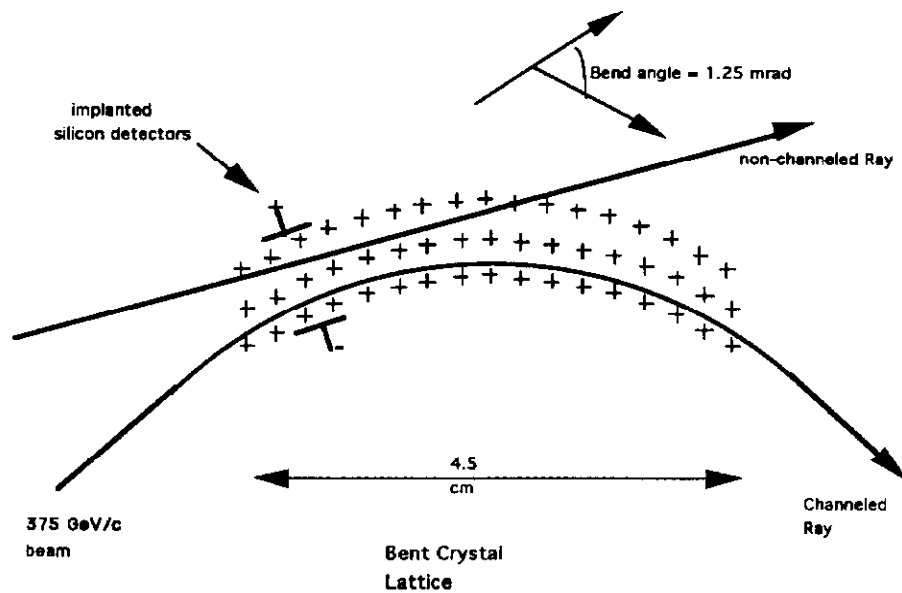


**Figure 17**  
E761 crystal setup for channeling

Figure 17 schematically shows the crystal configuration used in E761. In the actual experiment two crystals of silicon were placed (one bending up and the other down) in a 375 GeV/c beam which contained about 1%  $\Sigma^+$  (the rest being mainly protons and  $\pi^+$ ). This crystal was also implanted with solid state energy loss detectors so that the energy deposited in the crystal could be measured for each incident particle. Apparatus upstream (not shown) of the crystal measured the incident particle momentum and angle (with a precision of  $\approx 0.2\%$  and  $\approx 10 \mu\text{rad}$  respectively). A downstream spectrometer (also not shown) measured the particle momentum and trajectory a second time. Figure 18 shows some results<sup>39</sup> where no distinction is made between particle types. Thus it contains mostly protons and  $\pi^+$ . Figure 18a shows the difference between the angle measured entering and exiting the crystal. Peaks at  $\approx \pm 1.65 \text{ mrad}$  correspond to the known bending angles of the two crystals.

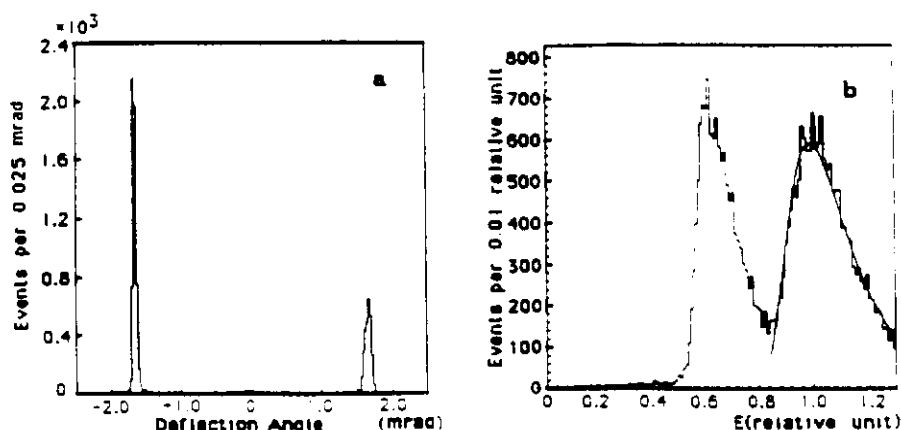


Figure 18

- (a) Deflection of beam by crystals.
- (b) Energy loss for incident particles.

Another characteristic is that the channeled particles lose less energy due to ionization than their non-channeled counterparts. Figure 18b shows the energy deposition in the crystal for those events which triggered<sup>39</sup> the apparatus. The peak at lower energy loss values is due to channeled particles. The solid line through the non channeled portion is a theoretical Landau distribution.



In this experiment the spin precession of channeled particles in bent crystals has been observed<sup>39</sup> for the first time. These crystals provided an effective magnetic field of 45 T which resulted in a measured spin precession of  $60 \pm 17^\circ$ . This agrees with the prediction of  $62 \pm 2^\circ$  using the world average<sup>1</sup> of  $\Sigma^+$  magnetic moment measurements. This new technique gives a  $\Sigma^+$  magnetic moment of  $2.40 \pm 0.46 \pm 0.40 \mu_N$  where the quoted uncertainties are statistical and systematic respectively. No evidence of depolarization in the channeling process was seen.

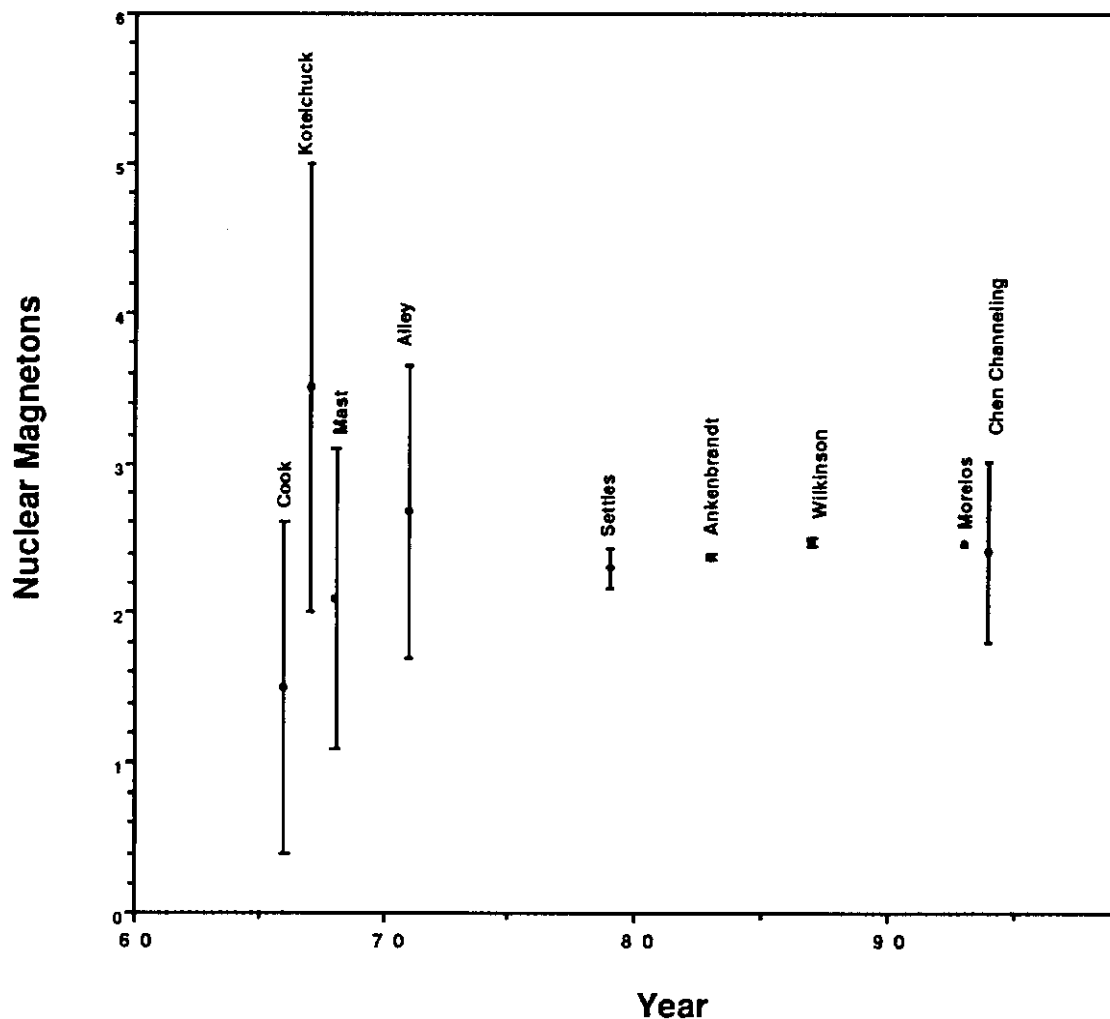


Figure 19  
History of  $\Sigma^+$  Magnetic Moment Measurements

The crystal bend angle of 1.65 mrad was chosen to match the acceptance of the downstream spectrometer. The crystal was bent to angles as large as 10 mrad (without breaking!) which would correspond to an effective magnetic field of  $\approx 275$  T.

Figure 19 shows the history of  $\Sigma^+$  magnetic moment<sup>40-44,14,15,32</sup> measurements. Note that in the early 1970's this would have been the most precise measurement of the  $\Sigma^+$  magnetic moment.

An exciting possibility is the application of this technique to charmed baryons which have a much shorter lifetime<sup>1</sup> than  $\Sigma^+$ . Note that at 500 GeV/c the  $\Lambda_c^+$  and  $\Xi_c^+$  would have decay lengths of 1.2 and 2.6 cm respectively.

The phenomena of hyperon polarization in high energy interactions has forced us to rethink the basic physics of these processes. It has also provided us with a very precise tool to measure hyperon magnetic moments.

I would like to acknowledge many important discussions with my Fermilab hyperon colleagues. This work is supported by the U.S. Department of Energy under contract DE-AC02-76CH03000.

### References

1. Particle Data Group, Phys. Rev. **D45**, 1 (1992).
2. J. Lach and L. Pondrom, Annu. Rev. Nucl. Part. Sci. **29**, 203 (1979).
3. L. Pondrom, Phys. Rep. **122**, 57 (1985).
4. J.M. Gaillard and G. Savage Ann. Rev. Nucl. Part. Sci. **34**, 351 (1984).
5. M. Bourquin and J.P. Repellin, Phys. Reports **114**, 100 (1984).
6. T.R. Cardello *et al.*, Phys. Rev. **32**, 1 (1985).
7. M. Foucher *et al.*, Phys. Rev. Lett. **68**, 3004 (1992).
8. V. Hungerbuhler *et al.*, Phys. Rev. **D12**, 1203 (1975).
9. J. Badier *et al.*, Phys. Lett. **39B**, 414 (1972).
10. K.B. Luk *et al.*, Phys. Rev **D38**, 19 (1988).
11. G. Bunce *et al.*, Phys. Rev. Lett. **36**, 1113 (1976).
12. K. Heller *et al.*, Phys. Rev. Lett. **41**, 607 (1978).
13. Basel Convention Helv. Phys. Acta Suppl. **VI**, (1961).

14. C. Ankenbrandt *et al.*, Phys. Rev. Lett. **51**, 863 (1983).
15. C. Wilkinson *et al.*, Phys. Rev. Lett. **58**, 855 (1987).
16. Y.W. Wah *et al.*, Phys. Rev. Lett. **55**, 2551 (1985).
17. L. Deck *et al.*, Phys. Rev. **D28**, 1 (1983).
18. G. Zapalac *et al.*, Phys. Rev. Lett **57**, 1526 (1986).
19. R. Rameika *et al.*, Phys. Rev. **D33**, 3172 (1986).
20. L.H. Trost *et al.*, Phys. Rev. **D40**, 1703 (1989).
21. H.T. Diehl *et al.*, Phys. Rev. Lett. **67**, 804 (1991).
22. P.M. Ho *et al.*, Phys. Rev. Lett. **65**, 1713 (1990).
23. A. Morelos *et al.*, Phys. Rev. Lett. **71**, 2172 (1993).
24. J. Szwed, Phys. Lett. **105B**, 403 (1981).
25. P. Cea *et al.*, Phys. Lett. **209B**, 333 (1988).
26. J. Soffer and N.A. Tornqvist, Phys. Rev. Lett. **68**, 907 (1992).
27. W.G.D. Dharmaratna and G.R. Goldstein, Phys. Rev. **41**, 1731 (1990).
28. B. Andersson *et al.*, Phys. Lett. **85B**, 417 (1979).
29. T.A. DeGrand and H.I. Miettinen, Phys. Rev. **24**, 2419 (1981).
30. R. Barni *et al.*, Phys. Lett. **B296**, 251 (1992).
31. P. Kroll, High Energy Spin Physics, Minneapolis, Minnesota, p 48, American Institute of Physics Conference Proceedings No. 187 (1988).
32. A. Morelos *et al.*, Submitted to Phys. Rev. Lett. (1993).
33. R. Rameika *et al.*, Phys. Rev. Lett. **52**, 581 (1984).
34. J. Duryea *et al.*, Phys. Rev. Lett. **68**, 768 (1992).
35. K. Johns *et al.*, Tenth International Symposium on High Energy Spin Physics, Nagoya, Japan, p (1992).
36. J. Franklin, Phys. Rev. **172**, 1807 (1968).
37. J.S. Forster *et al.*, Nucl. Phys. **B318**, 301 (1989).
38. R. Carrigan and J.A. Ellison, Relativistic Channeling (Plenum Press, New York, 1987).
39. D. Chen *et al.*, Phys. Rev. Lett. **69**, 3286 (1992).
40. V. Cook *et al.*, Phys. Rev. Lett. **17**, 223 (1966).
41. D. Kotelnichuk *et al.*, Phys. Rev. Lett. **25**, 1166 (1967).
42. T.S. Mast *et al.*, Phys. Rev. Lett. **23**, 1312 (1968).
43. P.W. Alley *et al.*, Phys. Rev. **D3**, 75 (1971).
44. R. Settles *et al.*, Phys. Rev. **D20**, 2154 (1979).